A COUPLED THERMO-MECHANICAL MODEL OF FRICTION STIR WELDING

by

Darko M. VELJIĆ [a], ***Milenko M. PEROVIĆ*** [b], ***Aleksandar S. SEDMAK*** [c*], ***Marko P. RAKIN*** [d], ***Miroslav V. TRIFUNOVIĆ*** [e], ***Nikola S. BAJIĆ*** [a], ***and Darko R. BAJIĆ*** [f]

[a] IHIS Science & Technology, Zemun, Belgrade, Serbia
[b] Chamber of Economy of Montenegro, Podgorica, Montenegro
[c] Faculty of Mechanical Engineering, University of Belgrade, Belgrade, Serbia
[d] Faculty of Technology and Metallurgy, University of Belgrade, Belgrade, Serbia
[e] Innovation Center of the Faculty of Mechanical Engineering, Belgrade, Serbia
[f] Faculty of Mechanical Engineering, University of Montenegro, Podgorica, Montenegro

Original scientific paper
DOI: 102298/TSCI110729012V

A coupled thermo-mechanical model was developed to study the temperature fields, the plunge force and the plastic deformations of Al alloy 2024-T351 under different rotating speed: 350, 400, and 450 rpm, during the friction stir welding process. 3-D FE model has been developed in ABAQUS/Explicit using the arbitrary Lagrangian-Eulerian formulation, the Johnson-Cook material law, and the Coulomb's Law of friction. Numerical results indicate that the maximum temperature in the friction stir welding process is lower than the melting point of the welding material. The temperature filed is approximately symmetrical along the welding line. A lower plastic strain region can be found near the welding tool in the trailing side on the bottom surface. With increasing rotation speed, the low plastic strain region is reduced. When the rotational speed is increased, the plunge force can be reduced. Regions with high equivalent plastic strains are observed which correspond to the nugget and the flow arm.

Key words: *thermo-mechanical model, temperature fields, plunge force, plastic deformations*

Introduction

Friction stir welding (FSW) is a solid state joining technique invented and patented in late 1991 by The Welding Institute (TWI). FSW is a process, in which specially shaped cylindrical tool is rotated and plunged into the abutting edges of the parts to be welded as shown in fig. 1. As the tool is moved along the joint line, the friction from the rotating tool heats the materials to the extent that it plastically deforms and flows from the front of the tool to the back, where it subsequently cools and produces a weld, *i*. *e*. weld is created by the combined action of frictional heating and mechanical deformation due to the rotating tool. The tool has a circular section except at the end where there is a threaded probe or more complicated flute, the junction between

* Corresponding author; e-mail: asedmak@mas.bg.ac.rs

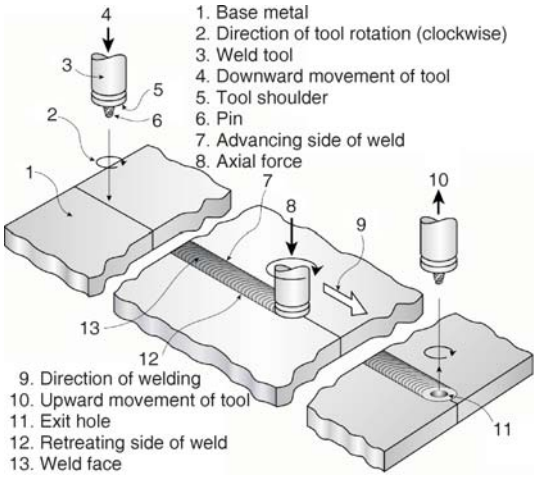

Figure 1. Schematic illustration of FSW process [1]

the cylindrical portion and the probe is known as the shoulder. The probe penetrated the welding plate, where as the shoulder rubs with the top surface. Use of FSW provides high quality welds, without voids, cracking.

Complex thermo-mechanical conditions exist in the near field matrix around the tool during the process which is categorized as thermo-mechanically affected zone (TMAZ) in the welding plate. This is also the zone that affects successful weld formation without a void. TMAZ is mostly in the plastic state and it is experimentally difficult to determine the temperatures in the welding plate due to large deformation of the material. Understanding of the complex thermo-mechanical conditions prevalent during the process in this zone can lead to better control of the weld formation process.

This paper investigates the linear welding phase using 3-D finite element (FI) model. A coupled thermo-mechanical 3-D FE model has been developed in ABAQUS/Explicit using the arbitrary Lagrangian-Eulerian formulation and the Johnson-Cook material law. The contact forces are modeled by Coulomb's Law of friction, making the contact condition highly solution dependent.

Table 1. Material properties of Al 2024 T351 [2, 3]

Material properties	Value
Young's modulus of elastic [GPa]	73.1
Poisson´s ratio	0.33
Initial yield stress [MPa]	270
Ultimate tensile strength [MPa]	410
Thermal conductivity [$Wm^{-1}K^{-1}$]	121
Coefficient of thermal expansion [$°C^{-1}$]	$24.7 \cdot 10^{-6}$
Density [kgm^{-3}]	2770
Specific heat capacity [$Jkg^{-1}°C^{-1}$]	875
Solidus [°C]	502
Liquids [°C]	638

Determination of the material properties

In the present work, material of the welding plate is Al 2024-T351. Chemical composition of 2024-T351 aluminum: Aluminum (Al) – balance, Cu – 4.52, Mg – 1.60, Mn – 0.65, Fe – 0.28, Si – 0.12, Zn – 0.09, Ti – 0.16, Cr – 0.01, other, total – 0.02% [1]. The thermal and mechanical properties used in this model are given in tab. 1. The material of the tool is steel 155CrVMo121. The material of the backing plate is steel 42CrMo4. The elastic-plastic Johnson-Cook material law provides the dependence of the current yield stress on plastic strain, plastic strain rate and temperature – see eq. (3). The influence of temperature on the material thermal properties is not pronounced in the case of FSW, because their change with temperature is not large.

Numerical analysis

Geometry and finite element mesh

The dimensions of the welding plate in the 3-D numerical model are 100 × 50 × 3 mm. Finite element C3D8RT [4] is used in the analysis; it is a thermo-mechanically coupled hexahedral element with 8-nodes, each having trilinear displacement and temperature degrees of freedom. This element produces uniform strain (first-order reduced integration) and contains hourglass control [5].

In order to get a reliable numerical result, detailed analysis has been conducted on different finite element meshes. In this paper, only the model which resulted in convergent solution is presented. The finite element mesh consists of 32298 nodes and 28522 elements. The tool and the backing plate are modeled as rigid surfaces having no thermal degrees of freedom. The tool has a conical pin and shoulder has a radius of 9 mm, fig. 2. The numerical model of welding plate, tool and backing plate is shown in fig. 3. The welding tool, which is used in numerical analysis, has a cylindrical pin and shoulder a radius of 3 and 9 mm.

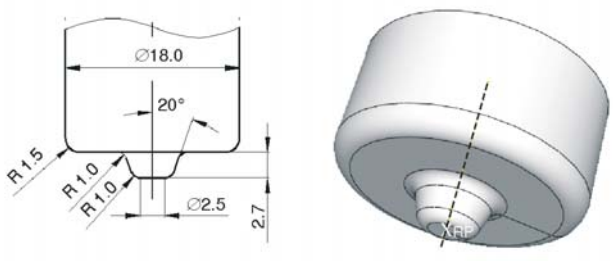

Figure 2. The welding tool which is used in experiment analysis

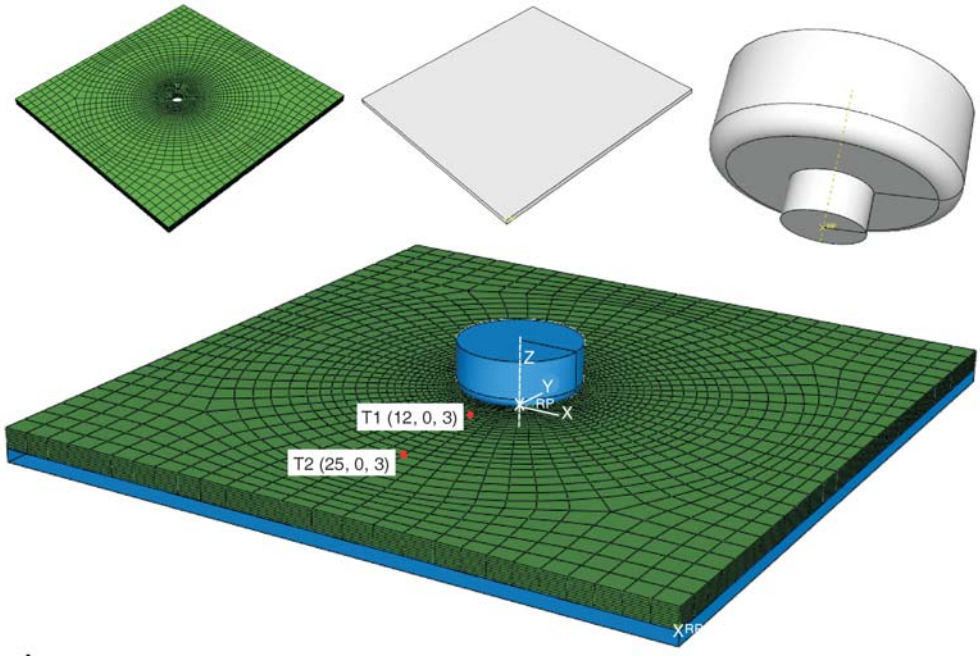

Figure 3. The numerical model of welding plate, tool and backing plate (color image see on our web site)

Governing equations for thermal analysis

In Abaqus/Explicit the heat transfer equations are integrated using the explicit forward-difference time integration rule [4]:

$$\theta_{i+1}^{N} = \Delta t_{i+1}\dot{\theta}_{i}^{N} + \theta_{i}^{N} \tag{1}$$

where θ^N is the temperature at node N and the subscript i refers to the increment number in an explicit dynamic step.

Governing equations for mechanical analysis

The equation of motion or mechanical response of the workpiece is given by [4]:

$$- p = \rho\vec{\mathrm{u}}'' + k\vec{\mathrm{u}} \tag{2}$$

where ρ is the density, k – the stiffness coefficient, p – the body force, and $\vec{\mathrm{u}}$ – the displacement vector.

Johnson-Cook elastic-plastic model

A temperature and strain rate dependent material law is implemented using the elastic-plastic Johnson-Cook material law [6]:

$$\sigma_y = [A + B(\varepsilon_p)^n]\left(1 + C\frac{\dot{\varepsilon}_p}{\dot{\varepsilon}_o}\right)\left[1 - \left(\frac{T - T_{\mathrm{romm}}}{T_{\mathrm{melt}} - T_{\mathrm{room}}}\right)^m\right] \tag{3}$$

where $T_{\mathrm{melt}} = 502$ °C is the melting point or solidus temperature, $T_{\mathrm{room}} = 20$ °C – the ambient temperature, T °C – the effective temperature, $A = 265$ MPa – the yield stress, $B = 426$ MPa – the strain factor, $n = 0.34$ – the strain exponent, $m = 1$ – the temperature exponent, and $C = 0.015$ – the strain rate factor. A, B, C, n, T_{melt}, T_{room}, and m are material/test constants for the Johnson-Cook strain rate dependent yield stress for Al 2024 T351 [3, 7].

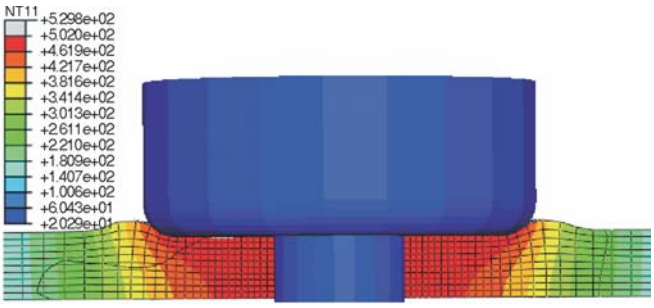

Figure 4. Temperature fields in the longitudinal cross-section after 1.0 s – step1, when rotation speeds is 350 rpm (color image see on our web site)

Results and discussion

Figure 4 shows the temperature fields in the longitudinal cross-section after 1.0 s – step1, when rotation speeds is 350 rpm. The welding speed is 120 mm per minute, and plunge depth is 0.2 mm. The heat transfer through the bottom surface of the workpiece is controlled by the heat transfer coefficient of 1000 W/m^{2}K. A constant friction coefficient of 0.3 is assumed between the tool and the workpiece and the penalty contact method is used to model the contact interaction between the two surfaces. Heat convection coefficients on the surface of the workpiece are $h = 10$ W/m^{2}K with the ambient temperature of 200 °C [8-9]. The temperature in

the matrix under the tool is in the range between 430 and 500 °C, which is lower than the melting temperature of the alloy 2024 T351. This transient temperature field is close to symmetrical and suitable for starting the longitudinal motion of the tool.

Figure 5 shows the temperature fields of the welding plate after 7.0 s and 10.0 s, in step 2 (weld period). The tool rotational speed is 350 rpm and plunge depth is 0.2 mm. The welding speed is 120 mm/min. The temperature filed is approximately symmetrical along the welding line.

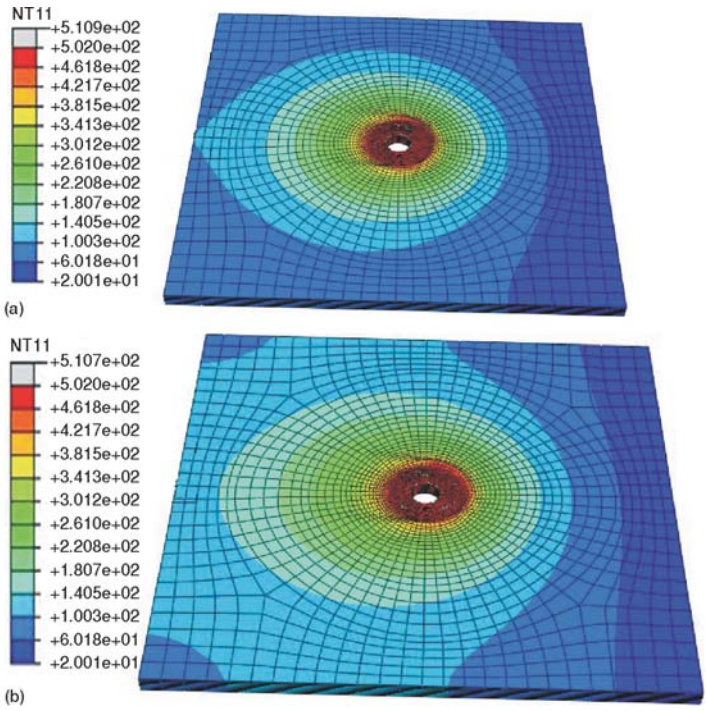

Figure 5. Temperature distribution in aluminum plate 2024-T351 after 7.0 s (a) and 10.0 s (b), in step 2 (weld stage) (color image see on our web site)

This can be seen by monitoring the progress in temperature for two nodes (fig. 6): the first node – T1 (12, 0, 0) is positioned beside the shoulder and the second node – T2 (25, 0, 0). Figure 3 shows the co-ordinates of points T1 and T2. In the first node the temperatures is stabilizes at ~380 °C after $t = 3$ s.

Figure 7 shows the plunge force during the FSW process for different rotating speed: 350, 400, and 450 rpm. After establishing of contact during the plunge period, a plunge force of 65 kN is observed. The force then drops as the material plasticises and softens under high stress and temperature increase. As the weld phase starts, the vertical force converges toward a steady-state condition. When the rotational speed is increased, the plunge force can be reduced.

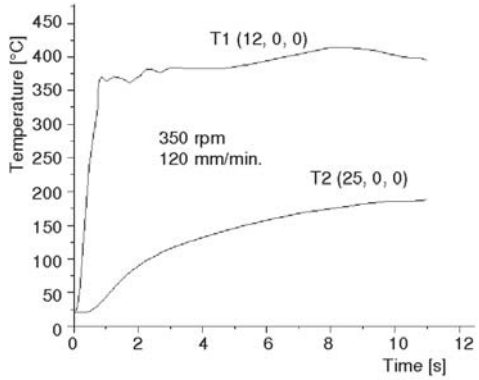

Figure 6. The temperature dependence of the time (point T1 and T2), plunge depth is 0.2 mm

Figure 8 shows the equivalent plastic strain fields in the longitudinal cross-sections for different rotating speed: 350, 400, and 450 rpm, after 10 s – step 2. The welding speed is 120 mm per minute, and plunge depth is 0.2 mm. The deformation of material near the top surface is larger than that near the bottom surface. There is

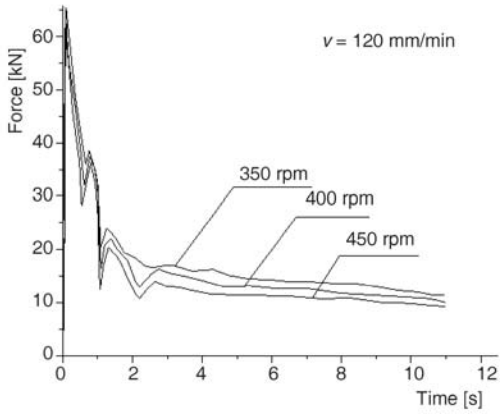

Figure 7. The force dependence of the time (rotation speeds v = 120 mm/min., plunge depth is 0.2 mm)

a lower plastic strain region on the bottom behind the tool in the trailing side [4]. With increasing rotation speed, this region is reduced.

Figure 9 shows microstructure in the transverse cross-section. The black line indicates the extent of the flow arm and nugget, which are comparable with the regions with high equivalent plastic strain shown in fig. 10. The equivalent plastic strain is increased on the advancing side. Advancing side to the right and retreating side to the left. The advancing side of the weld is defined as the side on which the rotational velocity vector of the welding tool has the same sense as the translational velocity vector of the tool relative to the workpiece. The retreating side is where the two vectors are of opposite sense [10].

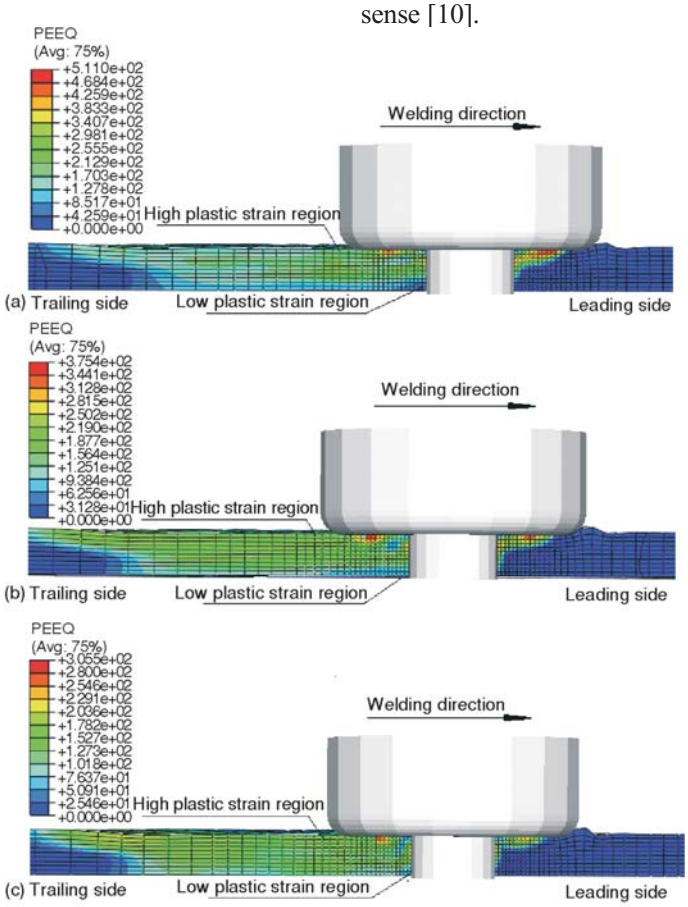

Figure 8. Equivalent plastic strain fields in the longitudinal cross-sections under varying rotational speeds: (a) 350 rpm, (b) 400 rpm, (c) 450 rpm, after 10 s – step 2 (color image see on our web site)

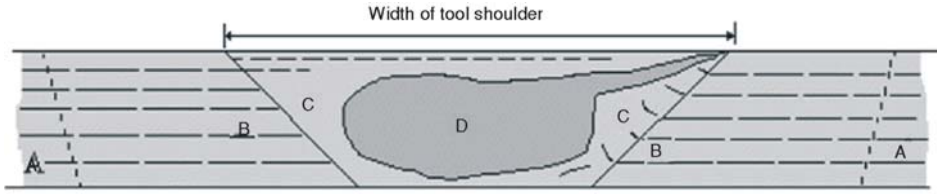

Figure 9. Microstructure in the transverse cross-section [11]

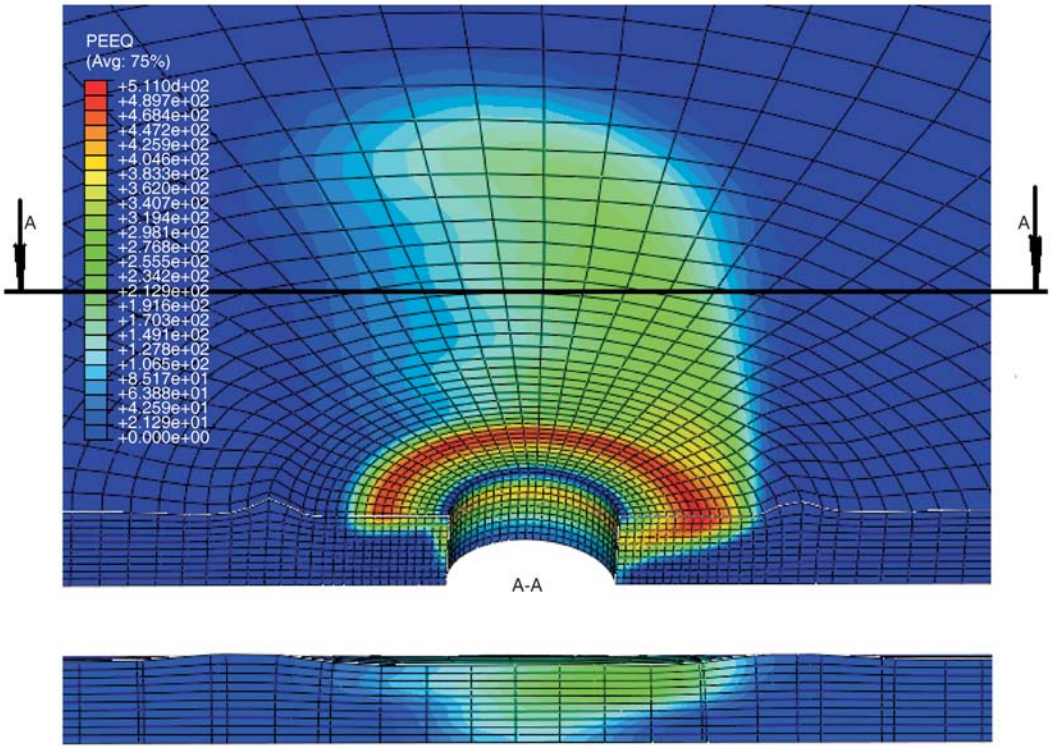

Figure 10. Equivalent plastic strain fields in the transverse cross-section. Advancing side to the right and retreating side to the left. (rotation speeds 350 rpm, plunge depth is 0.2 mm, welding speed v = 120 mm/min) (color image see on our web site)

Conclusions

The temperature fields, plunge force, and plastic deformations of Al alloy 2024-T351 under different rotating speeds during the (FSW) process were analysed using a coupled thermo-mechanical finite element model. Main conclusions obtained in this study are summarized:

- The temperature in the matrix is lower than the melting temperature.
- The temperature field is approximately symmetrical along the welding line.

- When the rotational speed is increased, the plunge force can be reduced.
- A lower plastic strain region can be found near the welding tool in the trailing side on the bottom surface.
- With increasing rotation speed, the low plastic strain region is retreating.
- The equivalent plastic strain is increased on the advancing side in comparison with the returning side.

References

[1] ***, An American National Standard, AWS D17.3/D17.3M:200X, American Welding Society "Specification for Friction Stir Welding of Aluminum Alloys for Aerospace Hardware" http://ampcenter.sdsmt.edu/docs/D17-3%20FSW%20Draft%2016%20bolser%201-22-0908032009.pdf
[2] ***, Aluminum 2024-T4; 2024-T351 – ASM Materal Data Sheet, http://asm.matweb.com/search/Specificmaterial.asp?bassnum+MA2024T4
[3] Johnson, G. R., Cook, W. H., A Constitutive Model and Data for Metals Subjected to Large Strains, High Rates and High Temperatures, *Proceedings,* 7th International Symposium on Ballistics, Hague, The Netherlands; 1983, pp. 541-547
[4] ***, Abaqus Inc., Analysis – User's Manual v. 6.7, 2007
[5] Zhang, Z., Bie, J., Zhang, H., Effect of Traverse/Rotational Speed on Material Deformations and Temperature Distributions in Friction Stir Welding, *J. Mater. Sci. Technol., 24* (2008), 6, pp. 907-914
[6] Veljić, D., *et al*., Numerical Simulation of the Plunge Stage in Friction Stir Welding, *Structural Integrity and Life, 11* (2011), 2, pp. 131-134
[7] Veljić, D., *et al*., Thermo-Mechanical Modeling of Friction Stir Welding, *Proceedings on CD*, 4th International Conference Innovative Technologies for Joining Advanced Materials, Timisoara, Romania, 2010, pp. 171-176
[8] Schmidt, H., Hattel, J., A Local Model for the Thermo Mechanical Conditions in Friction Stir Welding, *Modelling Simul. Mater. Sci. Eng., 13* (2005), 1, pp. 77-93
[9] Ivanović, I. B., *et al*., Numerical Study of Transient Three-Dimensional Heat Conduction Problem with a Moving Heat Source, *Thermal Science, 15* (2011), 1, pp. 257-266
[10] ***, http://www.twi.co.uk/ Microstructure Classification of Friction Stir Welds
[11] Veljić, D., Technology of Friction Stir Welding of Aluminum Alloys, M. Sc. Thesis, Faculty of Mechanical Engineering, University of Belgrade, Belgrade, Serbia, 2006

Paper submitted: July 27, 2011
Paper revised: January 6, 2012
Paper accepted: January 30, 2012